Supplementary Information for "Memory and recovery effects in the strain hardening regime of glassy polymers : theory and simulations"

Thomas C. Merlette[1,2], Jérôme Hem[1], Caroline Crauste-Thibierge[1], Sergio Ciliberto[1], Jérôme Bikard[3], Didier R. Long[2,**,†]

†1 1 *Univ Lyon, ENS de Lyon, CNRS, Laboratoire de Physique, F-69342 Lyon, France*

‡2 *Univ Lyon,CNRS, INSA Lyon, Université Claude Bernard Lyon 1, MATEIS, UMR5510, 69100 Villeurbanne, France*

¶3 *Solvay, RICL, 87 avenue des Frères Perret, 69192 Saint Fons Cedex, France*

E-mail: didier.long@insa-lyon.fr

I. Additional simulation results

In this section, additional simulation results are displayed where some model parameters values were changed (μ_2 and $\frac{1}{R}$) or the waiting time was increased (up to 100 s). The simulations presented in this section were performed with a time step $\delta t = 10^{-3}s$, whereas the value of $\delta t = 10^{-4}s$ was used for all other simulations in the current manuscript.

I.1. Influence of model parameters μ_2 and $\frac{1}{R}$

Figure S1 shows simulation results during protocol II with different values for parameters μ_2 and $\frac{1}{R}$, where the waiting step was performed at $\varepsilon_0 = 0.75$. In (a), stress-strain curves during the second tension are plotted whereas in (b), the time evolution of $< Tr\left(\underset{\sim}{q}^2\right) >$ (normalized) during the waiting step is displayed. Note that in (b), the relative average orientation is plotted instead of the average orientation itself, so that the different curves start from 1 and can be compared on the same graph. The waiting step lasts for 10s.

μ_2 relates orientation to the free energy barrier increase according to equation 7, whereas $\frac{1}{R}$ sets the restoring force which drives orientation back to zero as in equations 7 of the manuscript. As discussed in,[1] strain hardening during a uniaxial tension or compression performed on an isotropic system is less pronounced when either μ_2 decreases or $\frac{1}{R}$ increases. It can be seen on figure S1 (a) that in this case, strain hardening is less pronounced also during the second tension of protocol II. The reference values $\mu_2 = 300$ and $\frac{1}{R} = 0.1$ (black curve) were used for simulations presented in the current manuscript as well as in[1] unless specifically stated.

For the sets of parameters $\{\mu_2 = 100, \frac{1}{R} = 0.1\}$ and $\{\mu_2 = 300, \frac{1}{R} = 0.17\}$, no strain hardening is observed as can be seen in figure S1 (a). Those correspond to the only two situations where average orientation relaxes during the waiting step among the displayed results (figure S1 (b)): $< Tr\left(\underset{\sim}{q}^2\right) >$ relaxes by about 25% for $\frac{1}{R} = 0.17$ and 40% for $\mu_2 = 100$ and would continue to slightly decrease if the waiting step lasted longer. However, it must be noted that the values of $< Tr\left(\underset{\sim}{q}^2\right) >$ at the beginning of the waiting

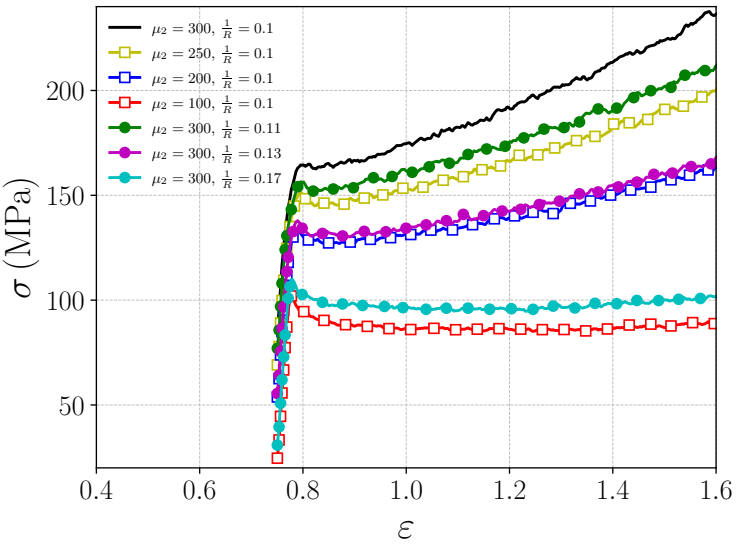

(a)

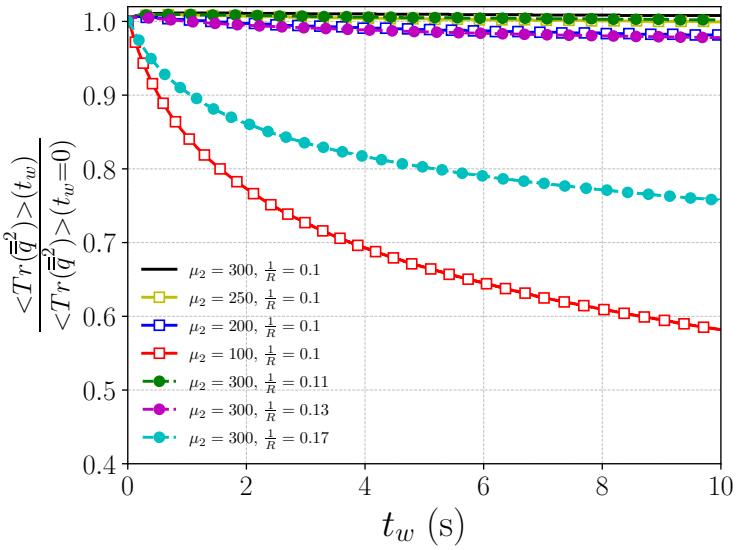

(b)

Figure S1: (a) Evolution of stress as a function of strain during the second tension of protocol II, i.e. after a first tension up to a given prestrain $\varepsilon_0 = 0.75$ followed by a 10 seconds waiting step. (b) Evolution of average orientation (normalized with the initial value) with waiting time t_w during the waiting step. The tensile test simulations are performed at 345 K and 0.1 s^{-1} along the same direction. Several curves are plotted, corresponding to different values of μ_2 (curves with open square symbols) and $\frac{1}{R}$ (curves with solid circle symbols). The black curve corresponds to the one with the "standard" values $\mu_2 = 300$ and $\frac{1}{R} = 0.1$. The 2 curves showing orientation relaxation (red and cyan) correspond to low initial values of $< Tr\left(\underset{\sim}{q}^2\right) >$, for which no strain hardening occurs.

step, not displayed here, are very low ($\sim 2.5\,10^{-3}$ for $\mu_2 = 100$ and $\sim 2\,10^{-3}$ for $\frac{1}{R} = 0.17$).

Strain hardening and orientation relaxation during the waiting step are thus strongly correlated. Whenever the parameters lead to strain hardening, $< Tr\left(\underset{\sim}{q}^2\right) >$ does not relax (or not significantly) during the waiting step. This quantity only relaxes when no or very little strain hardening is observed. This is due to strain hardening being the consequence of a fraction of highly-oriented regions whose internal dynamics is significantly slowed down. Whenever the model parameters enable Kuhn segments orientation to take place for a large enough fraction of subunits, strain hardening occurs as explained in.[1] At this point, orientation does not relax "by itself" in those regions during the waiting step because the facilitation mechanism is no longer effective, as explained in section IV of the current manuscript. On the other hand, considering a situation where orientation indeed relaxes during the waiting step requires the local free energy barriers to be only poorly increased (or not increased at all) by local orientation: in this case, strain hardening does not occur (or has not occurred yet).

Therefore, the theory predicts that orientation $< Tr\left(\underset{\sim}{q}^2\right) >$ does not relax within experimental timescales whenever strain hardening is observed. It does relax when strain hardening is absent, but in this situation the theory predicts that the average value of Kuhn segment orientation is very small. The parameter range in which strain hardening occurs and orientation relaxes within the experimental time frame, if it exists, is very narrow

and hard to identify.

I.2. Influence of a large waiting time

In the core manuscript, no (or very slight) overshoot was observed for tanδ. Such an overshoot can be observed in experiments when the waiting time is large enough, and is more evident when the waiting step takes place at small strain values.[2]

Simulations were run with a waiting step that lasted for 100s at 2 different strain values, 25% and 50%, with the reference values for model parameters ($\mu_2 = 300$ and $\frac{1}{R} = 0.1$). Results are displayed in figure S2. The evolution of stress (a), $\left\langle Tr(\underset{\sim}{q}^2) \right\rangle$ (b) and tan(δ) (c) are plotted as a function of strain during the entire protocol (except for the waiting step which is only displayed in (a)).

Description of subfigures (a) and (b) does not differ from that of figures 6 (a) in the manuscript and figure S1 of the SI: the stress overshoot is very pronounced here because the system could age significantly during the long waiting step, and orientation does not relax during this waiting step.
In figure S2 (c), tan(δ) during the second tension overshoots the reference curve (i.e. without the waiting step), especially for small strain values ε_0 at which the waiting step is performed. The overshoot is clear for $\varepsilon_0 = 0.25$, it is less pronounced (but still exists) for $\varepsilon_0 = 0.5$ and it is very slight for $\varepsilon_0 = 0.75$. It is probable that if the waiting time was larger (say 1000s), the overshoot would be more pronounced and that one could also be observed at very higher strain values such as 0.75.

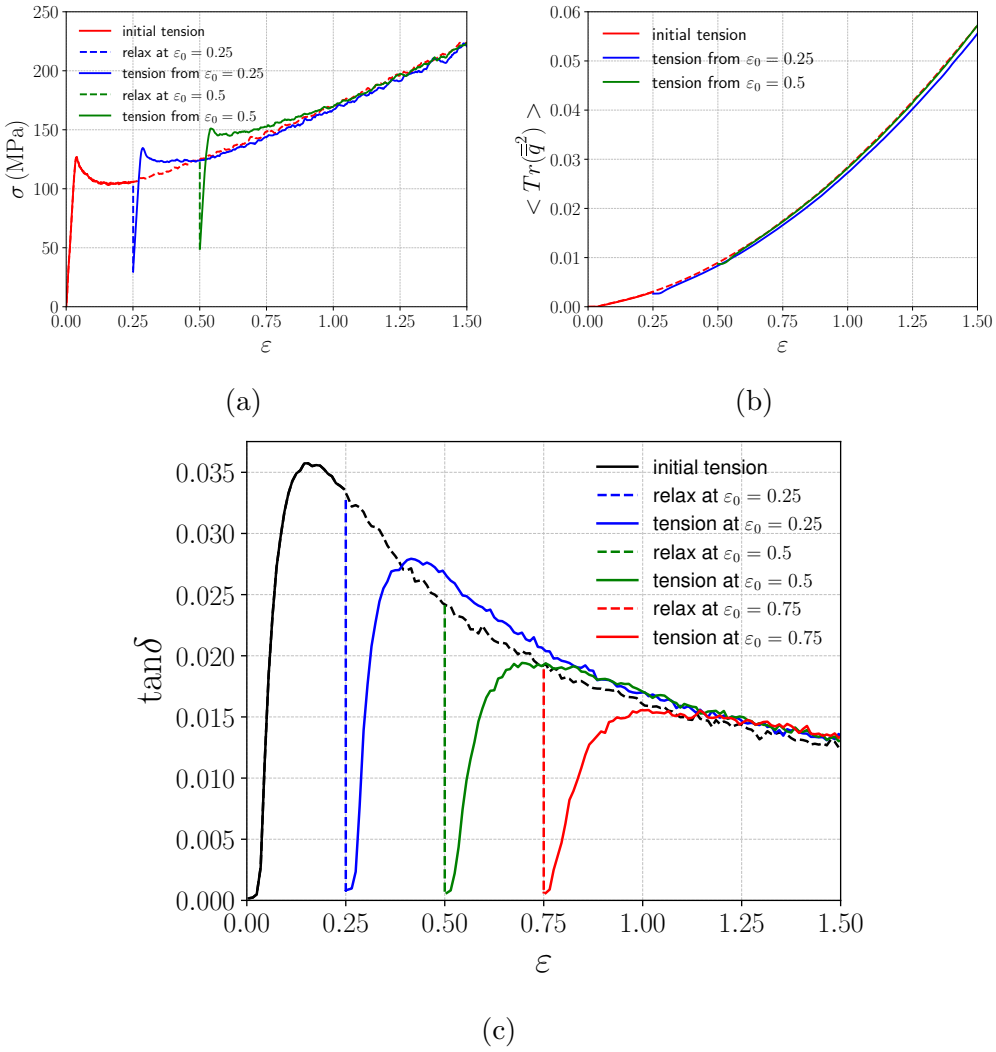

Figure S2: (a) Evolution of stress (a), average orientation (b) and tanδ (c) as a function of strain during the second tension of protocol II. The different curves correspond to different strain values ε_0 where a waiting step of 100s was performed ($\varepsilon_0 = 0.25$, 0.5 and 0.75). The reference parameters values are used ($\mu_2 = 300$ and $\frac{1}{R} = 0.1$). Simulations were performed with a time step of $\delta t = 10^{-3}$s.

Therefore, the theory can predict also an overshoot for the dynamical response (tan(δ)) which is due to the significant aging of the glassy polymer during the waiting step.

I.3. Evolution of the relaxation times distribution before strain hardening

The evolution of the DRT (distribution of relaxation times) presented in Figure 2b shows a pronounced change between the initial stage ($\varepsilon = 0$) and the onset of strain hardening (approximately $\varepsilon = 0.25$). In Figure S3 below, we provide additional distributions at intermediate strain levels.

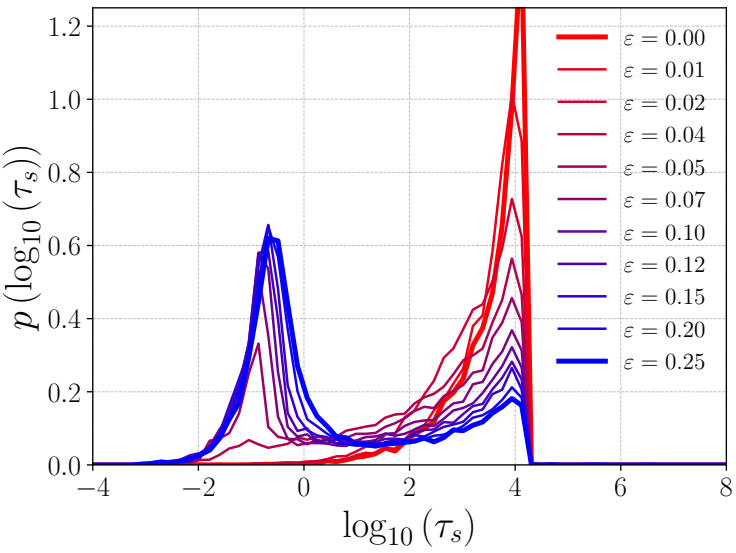

Figure S3: Distribution of relaxation times at different strain values up to the onset of strain hardening, during a uniaxial tension at a constant strain rate. Note that the 2 extreme curves ($\varepsilon = 0$ and $\varepsilon = 0.25$) are plotted in bold and have the same colors as in Figure 2b.

II. System representation

In this section, we describe briefly the numerical model which was developed in previous works in order to solve numerically the equations of the theoretical model in three dimensions.[1,3–7] much of this section has already been described in the SI section of.[1] The numerical values of the quantities are reported in Table 1.

II.1 Interacting objects and forces

The numerical system is represented by a 3D simulation box containing **nodes** connected together via 2 different types of springs : **glassy springs**, which model dynamical heterogeneities (also called subunits in the current manuscript), and **rubbery springs**, which model the elasticity of the entangled or cross-linked matrix. An illustration of the simulation box is shown in Figure S4.

Three types of forces are acting on nodes:

- Hard core repulsion between nodes :

$$\vec{F}_{HS}(r) = \begin{cases} 12\frac{u_0}{r}\left(\frac{d}{r}\right)^{12}\frac{\vec{r}}{r} + F_{reg}(r)\frac{\vec{r}}{r} \text{ if } \ r < r_{HS} \\ 0 \text{ if } \ r > r_{HS} \end{cases}$$

  with $F_{reg}(r)$ a regularisation term for a smooth evolution of $\vec{F}_{HS}(r)$ around r_{HS}. r is the distance between the two nodes.

- Elasticity of rubbery springs :

$$\vec{F}_r = -k_\infty \left(r - l_0\right) \vec{u}_r$$

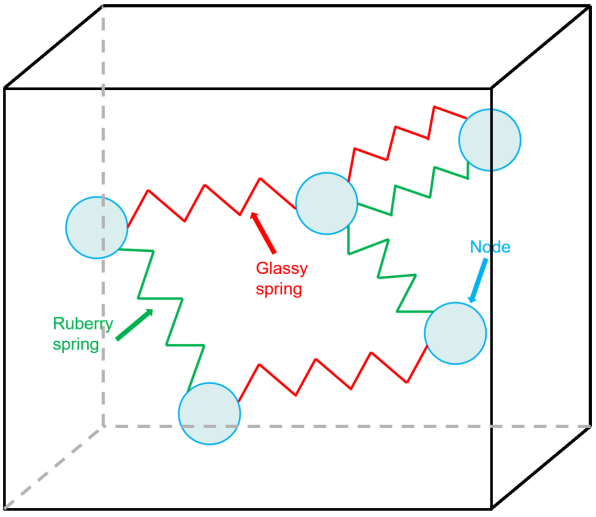

Figure S4: The figure is reproduced from.[1] It is an illustration of the different objects inside the simulation box (the number of objects, scales and springs connectivity are obviously not respected). Glassy and rubbery springs are connected through nodes. Nodes are the moving objects : periodic boundary conditions are applied with the so-called minimum image convention. Glassy springs are the objects of interest since they model the subunits (dynamical heterogeneities) of length 3-5 nm.

where $\vec{F}_r$ is the force exerted by node B on node A (if connected by a rubbery spring), $\vec{u}_r$ is the unit vector from A to B, r the spring length and l_0 the equilibrium length of the rubbery spring. l_0 is a constant of the order of ξ.

- Elasticity of glassy springs :

$$\vec{F}_g = -k_0 \left(\vec{r^g} - \vec{r_0^g} \right)$$

where $\vec{F}_g$ is the force exerted by node B on node A (if connected by a glassy spring), $\vec{r^g}$ is the *position vector* of the glassy spring from node A to node B ($\vec{r^g} = \vec{AB}$) and $\vec{r_0^g}$ is the *equilibrium position vector* of the glassy spring.

The connectivity (average number of springs per node) has been set to 7 for glassy springs and 12 for rubbery springs, consistently with.[1,5] In this manuscript, the numerical systems for the simulations are composed of 3375 nodes, 12030 glassy springs and 20250 rubbery springs, corresponding to the same values as in.[1] The glassy springs are the relevant ingredients below T_g, thus the system comprises roughly $12030 \times 3 \approx 36000$ degrees of freedom. Note that the system is sufficiently large for the numerical results to be essentially insensitive to the box size; further increases would only reduce numerical noise.

The objects of interest are glassy springs which model subunits. Those springs can relax the stress they bear: they possess an unusual behavior which is described below.

II.2 Local and global stress

The local glassy stress tensor $\underset{\sim}{\sigma}^g$ associated with a glassy spring is given by : $\sigma^g_{ij} = \frac{F_{g,i}.r^g_j}{2\,\xi^3}$ where $F_{g,i} = \vec{F}_g.\vec{e}_i$ and $r^g_j = \vec{r}^g.\vec{e}_j$. This local glassy stress tensor is then symmetrized. Similarly, a local rubbery stress tensor $\underset{\sim}{\sigma}^r_{ij}$ is associated with a rubbery spring.

The local stress acting on a node is given by Irving Kirkwood's formula applied to a local volume of $2\,\xi^3$: $\sigma^{node}_{ij} = \frac{1}{2\xi^3}.\sum_k F^{(k)}_i.r^{(k)}_j$, with $F^{(k)}_i$ the i^{th} component of the force exerted by the spring k on the node, and $r^{(k)}_j$ the j^{th} component of the position vector of the spring k (the spring being either glassy or rubbery). It amounts to summing up glassy and rubbery stresses

associated with the springs connected to the considered node.
Note that $k_0 \gg k_\infty$, therefore the contribution to stress of glassy springs is much higher than that of rubbery springs if those glassy springs are not short-lived (i.e. if their relaxation time is not too low).

Global stress $< \sigma >$ is calculated according to Irving-Kirkwood's formula: $< \sigma_{ij} >= \frac{1}{2V}. \sum_{m,n} F_i^{(m,n)}.r_j^{(m,n)}$ where the summation runs over all pairs of nodes (i,j), with V the total volume of the simulation box, $F_i^{(m,n)}$ the i^{th} component of the force and $r_j^{(m,n)}$ the j^{th} component of the position vector between nodes i and j. This is equivalent to taking the average of the local nodal stresses.

II.3 Behaviour of the glassy springs

The numerical system deals with 12030 glassy springs, each having their own age t, stress tensor $\underset{\sim}{\sigma}$, relaxation time τ_s and order parameter $\underset{\sim}{q}$.

II.3.1 Local relaxation time

The local intrinsic relaxation time of a glassy spring τ_s is given by : $\tau_s = \frac{dt}{dP_{rel}}$, where dP_{rel} is the probability that the spring relaxes during dt, given by equation 7 of the article. The distribution of relaxation times $\{\tau_s\}$ is computed during the simulation at any time step, it numerically consists of a set of 12030 relaxation times. The effective local relaxation time of a given subunit is then given by $\tau_{\text{eff}} = \min(\tau_s, \tau_d)$, with τ_s the intrinsic relaxation time of the considered spring and $\tau_d = N_c^{\frac{2}{3}} \tau_f$ the diffusion time. The relaxation time τ_f of the 30 % fastest subunits (equation (5) of the article

with $q_c = 0.3$) is accessed numerically from the set of intrinsic relaxation times $\{\tau_s\}$.

One can note that the macroscopic rigidity of the system comes from the simulations and is not presupposed a priori.

II.3.2 Relaxation and aging mechanisms

The dependence of the intrinsic relaxation time τ_s of a glassy spring on its age t_w is given by Equation (6) of the article (with $\tau_s(t_w) = \frac{dt}{dP_{rel}(t_w,0,0)}$). τ_s is approximately proportional to the age t_w at a fixed temperature, with t_w the elapsed time since the last relaxation of the considered spring. Whenever the spring does not relax, its age t_w then increases like the elapsed time. Whenever the spring relaxes, its new equilibrium position vector becomes the current position vector ($\vec{r}_0^{\,g} \leftarrow \vec{r}^{\,g}$), therefore the local glassy force drops to zero, and the spring age also drops to a minimum value close to zero ($\delta t = 10^{-4}\, s$) hence τ_s tends to drop as well as a consequence. This enables to model ageing and rejuvenation of the glassy polymer.

The dependence of the relaxation time on temperature is given by the WLF law of the considered polymer. Below T_g, the global stress $< \sigma >$ comes from glassy springs which are long-lived.

II.3.3 Local orientation

The local order parameter $\underset{\sim}{q}$ is attached to a given glassy spring and evolves according to Equation (3) of the manuscript, where τ is the effective local relaxation time of the glassy spring ($= \tau_{\text{eff}}$ as defined previously) and $\underset{\sim}{\sigma}_{dev}$ the deviatoric local stress attached to the spring ($\underset{\sim}{\sigma}^g_{dev}$ as defined in the

current SI).

II.4 Numerical values of physical quantities and simulation procedures

II.4.1 Initialization

Table 1 presents the main simulation parameters with their numerical values as well as the corresponding physical quantities.
This step enables to create a simulation box with 3375 nodes bounded together with 12030 glassy springs and 20250 rubbery springs, such that the system is at mechanical equilibrium (nil internal stress and nodes velocities). The system then ages for a given given time ($10^4 s$ in our simulations) to let the distribution of relaxation times evolve according to time and temperature.

II.4.2 Simulation procedure for protocol II

The simulation procedure is described below. It is also written in pseudo code in algorithm 1 with t_1 and t_3 chosen to match the predefined strain values, $t_2 = 30\,s$ and $\vec{r}_0^{\,g}$ and $\vec{r}^{\,g}$ the equilibrium and current glassy spring vectors respectively.

1. Initially : distribution of ages $\{t\}$ (hence of relaxation times $\{\tau_s\}$ and $\{\tau_{\text{eff}}\}$) due to preliminary aging, distribution of nil glassy stresses and orientations ($\{\underset{\sim}{\sigma}^g\} = \{\underset{\sim}{q}\} = \{\underset{\sim}{0}\}$).

2. A tensile test is performed by applying a constant strain rate $\langle\dot{\varepsilon}\rangle = 10^{-1}s^{-1}$ to the system until the chosen predefined true strain $\langle\varepsilon_0\rangle$ is

Table 1: Main simulation parameters, with their corresponding physical quantities.

Simulation parameter	Physical equivalence	Numerical value
Thermal energy	$\sim k_B T_g$	~ 0.18
Unit length ξ	5 nm	1
Fast percolating fraction q_c	30%	0.3
Slow percolating fraction p_c	11%	0.11
Surface of a domain $N_c^{2/3}$	~ 100 monomers	10^2
Glassy stiffness k_0	$G_0\xi \sim 3\text{GPa} \cdot \xi$	~ 3000
Rubbery stiffness k_∞	$G'_\infty \xi \sim 10^5$ Pa $\cdot \xi$	~ 0.1
Plasticizing parameter λ	$\lambda \sim 10^{-15}\text{Pa}^{-2}$	10^{-3}
Orientation parameter μ_2	$\mu_2 \sim 300$	300
Pressure parameter a_p^*	$a_p \sim 0.01$	0.01 or 0
Entropic relaxation parameter $\frac{1}{R}$	$\frac{1}{R} \sim 0.1$	0.1
Average rubbery connectivity $g_{rubbery}$		12
Average glassy connectivity g_{glassy}		7
Excluded volume radius d	ξ	1
Excluded volume energy u_0	$(\sim \frac{1}{20} k_B T_g)$	~ 0.01
Equilibrium length of rubbery springs l_0	ξ	~ 1
Excluded volume cutoff r_{HS}	(3.26 nm)	1.08
Time step δt	10^{-4}s	10^{-4}
Poisson's ratio ν	0.5	0.5
	$C_1 = 16.0$	16.0
WLF parameters	$C_2 = 47.0K$	47.0
	$T_g = 370K$	365

reached along $\vec{e}_3$.

3. The system is maintained at this fixed $\langle \varepsilon_0 \rangle$ value for a given waiting time t_w (10 seconds in most simulations presented in the current manuscript).

4. Finally, the sample is deformed again in tension along $\vec{e}_3$ at the same initial strain rate $\langle \dot{\varepsilon} \rangle$ up to the predefined "final" total strain $\varepsilon_{\text{final}} = 1.5$.

The time step of the simulation is $\delta t = 10^{-4}\, s$ during the entire procedure.

An explicit Euler scheme is used in the simulations to solve the differential equations for the set of all nodes positions $\{\vec{r}\}$ and glassy springs orientations $\{\underset{\sim}{q}\}$.

1. Initial tension

$t_{\text{simu}} = 0$

while $t_{simu} < t_1$ **do**

1.1. Affine deformation :

Affine change of node positions : $\vec{r} \leftarrow (\underset{\sim}{I} + < \dot{\underset{\sim}{\varepsilon}} > .\delta t) .\vec{r}$

1.2. Explicit Euler Method:

Compute all variables at new time $t_{\text{simu}} \leftarrow t_{\text{simu}} + \delta t$

Update of global stress $< \underset{\sim}{\sigma} >$

1.3. Aging step :

for *all glassy springs* **do**

Compute τ_s

end

Compute τ_d

for *all glassy springs* **do**

Compute τ_{eff}

Compute rupture probability $\delta P_{\text{rel}} = \frac{\delta t}{\tau_{\text{eff}}}$

Compare δP_{rel} with random variable $v_{\text{rand}} \in [0, 1]$ (with uniform distribution) :

- $\delta P_{\text{rel}} < v_{\text{rand}} \rightarrow$ no relaxation : age $t \leftarrow t + \delta t$
- $\delta P_{\text{rel}} > v_{\text{rand}} \rightarrow$ relaxation : age $t \leftarrow t_{\min} = 2\delta t$ and spring equilibrium position $\vec{r}_0^{\,g} \leftarrow \vec{r}^{\,g}$

end

end

2. Waiting (relaxation) step during t_w

while $t_{simu} < t_1 + t_w$ **do**

Tension with $\dot{\varepsilon} = 0$ (same algorithm as 1. with no affine deformation)

end

3. Second mechanical test

while $t_{simu} < t_1 + t_w + t_2$ **do**

Tension at $\dot{\varepsilon}$ (same algorithm as 1.)

end

Algorithm 1: General algorithm of protocol II

BIBLIOGRAPHY

References

(1) Merlette, T. C.; Hem, J.; ; Crauste-Thibierge, C.; Ciliberto, S.; Clément, F.; Sotta, P.; Long, D. R. Theory of Plasticity and Strain Hardening of Glassy Polymers. *Macromolecules* **2023**, *56*, 6510–6526.

(2) Hem, J.; Merlette, T. C.; Crauste-Thibierge, C.; Clément, F.; Long, D. R.; Ciliberto, S. Microscopic Dynamics in the Strain Hardening Regime of Glassy Polymers. *Macromolecules* **2022**, *55*, 9168–9185.

(3) Dequidt, A.; Long, D. R.; Sotta, P.; Sanseau, O. Mechanical properties of thin confined polymer films close to the glass transition in the linear regime of deformation: Theory and simulations. *Eur. Phys. J. E* **2012**, *35*, 61.

(4) Dequidt, A.; Conca, L.; Delannoy, J.-Y.; Sotta, P.; Lequeux, F.; Long, D. R. Heterogeneous Dynamics and Polymer Plasticity. *Macromolecules* **2016**, *49*, 9148–9162.

(5) Conca, L.; Dequidt, A.; Sotta, P.; Long, D. R. Acceleration and Homogenization of the Dynamics during Plastic Deformation. *Macromolecules* **2017**, *50*, 9456–9472.

(6) Conca, L. *Mechanical properties of polymer glasses : Mechanical properties of polymer glasses, chapter 3, pages 81-90*; PhD thesis, Lyon, 2016.

(7) Merlette, T. C. *Theory of strain hardening of glassy polymers*; PhD thesis, Lyon, 2022.